Surface acoustic waves in a simple quasiperiodic system

Louis Macon,* Jean-Pierre Desideri, and Didier Sornette
Laboratoire de Physique de la Matière Condensée, Faculté des Sciences, Université de Nice, Parc Valrose, 06034 Nice CEDEX, France
(Received 7 March 1989)

We present experimental results and their interpretation on the propagation of surface acoustic waves on a particular one-dimensional quasiperiodically corrugated solid surface. This problem has previously been studied theoretically in the limit of a vanishing corrugation. We report precise results about the reflection and transmission frequency dependence, the temporal impulse response, and the spatial structure of the proper modes obtained from an optical diffraction experiment using the Raman-Nath effect (laser-beam diffraction by the surface ultrasonic deformations). The theoretical predictions are well observed experimentally. In particular, a special quasilocalized mode is observed which exhibits an interesting fine scale structure not predicted in the theory, since it falls outside its validity range. In the time domain, our experiments are able to clearly distinguish triple reflections and to count as many as 10^4 different paths which contribute coherently to the impulse time reflection signal.

I. INTRODUCTION

A lot of theoretical works[1,2] have been concerned with the propagation properties of quasiperiodic ($d=1$) lattices essentially focusing on the tight-binding discrete Schrödinger equation. On the experimental side,[3-6] a few works have been reported on semiconductor superlattices which have mainly focused on the study of their structural, dynamical, electronic, and optical properties in relation to the quasiperiodicity. The analog problem of acoustical or optical wave propagation in quasiperiodic lattices has been much less studied theoretically[7,8] and, to our knowledge, there are no experimental results in this field.

The problem of wave propagation in quasiperiodic systems is interesting since it is intermediate between periodicity and randomness. Another motivation for studying these systems follows from the recent experimental discovery of the quasicrystal phase in metallic alloys.[9] From a different point of view, studying the interaction of elastic surface acoustic waves with complex surface topography[10,11] is of major importance to underwater acoustics, seismology, surface acoustic wave devices, nondestructive testing, and ultrasonic applications in medicine. Quasiperiodic structures could also provide useful systems for analogical coding, multiband filters, random discretization, and integrated analogical frequency analyzer.

In this paper, we present experimental results and their interpretation on the propagation of Rayleigh-surface acoustic waves on a particular one-dimensional quasiperiodically corrugated solid surface. This problem has previously[1] been studied theoretically in the limit of a vanishing corrugation (implying a vanishing amplitude reflection coefficient $\mu \to 0$) in a large system of size L with $L^{-1/2} \ll \mu$ (see Sec. VI and Ref. 1 for an explanation of this inequality).

We report precise results about the reflection and transmission frequency dependence, the temporal impulse response, and the spatial structure of the proper modes obtained from an optical diffraction experiment. The theoretical predictions are well observed experimentally. The simple structure of our system offers interesting features which can be used as paradigms for more complicated systems. In particular, a striking quasilocalized mode is observed whose large scale shape is in good agreement with the theoretical model.[1] However, it also exhibits an interesting fine scale structure not predicted in Ref. 1 since it falls outside the validity range of the theoretical analysis. A second interest of our system lies in the analysis of the time response. Indeed, our experiments are able to distinguish clearly triple reflections and to count as many as 10^4 different paths which contribute coherently to the impulse time reflection signal. These results could be useful to improve present techniques based on ultrasonic acoustic wave propagation in more complex systems.[11]

The structure of the paper is the following. In Sec. II we present the experimental setup and recall some useful particularities of the surface acoustic waves which have been used. In Sec. III, we analyze the spectrum obtained from reflection and transmission studies. In Sec. IV, the spatial structure of some proper modes are reported and discussed. In Sec V, the time impulse response of the system is analyzed in detail. Section VI concludes by discussing some open problems and directions for the future.

II. EXPERIMENTAL SETUP

We have studied a lattice of identical grooves engraved at the surface of a piezoelectric lithium niobate (YZ-$LiNbO_3$) substrate, using well-known microlithographic techniques.[10] The system is represented in Fig. 1(a). Its construction is given as follows.[1] Let P and Q be two relatively prime numbers. The lattice of grooves is the superposition of two periodic lattices of period proportional

to P and Q. The groove density function is, therefore,

$$n(x)=\sum_m \delta(x-mPd_{\min})+\sum_n \delta(x-nQd_{\min}) . \quad (1)$$

It is periodic and the elementary cell contains $P+Q$ grooves. The system under study is made of one such elementary cell, with $P=F_{10}=89$, $Q=F_{11}=144$. The total number of grooves in the system is thus $N=P+Q=F_{12}=233$. F_n is the nth term of the Fibonacci series (generated iteratively by $F_{n+2}=F_{n+1}+F_n$, for $n\geq 2$, with $F_2=F_0=1$), which is such that the series of rational numbers F_n/F_{n+1} gives the most rapid convergence as $n\rightarrow+\infty$ to the irrational inverse golden mean $t=(\sqrt{5}-1)/2=0.6180\ldots$. The smallest spacing between two successive grooves is $d_{\min}=4$ μm which constitutes the unit length of the problem. The largest spacing is $d_{\max}=358.5$ μm and the mean spacing $a=221$ μm. The size of the system is $L=PQd_{\min}=F_{10}F_{11}d_{\min}=51\,264$ μm. Notice that the system is symmetric with respect to its center. The grooves have all the same well characterized profile [Fig. 1(b)] with a width $w=2$ μm and a depth $h=0.3$ μm. The lateral scale of each groove (the so-called opening) is $E=1860$ μm. In comparison, the typical wavelength of the surface acoustic waves (SAW's) is around 20 μm.

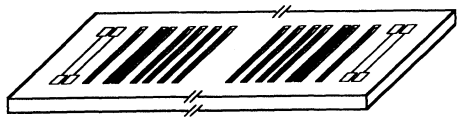

(a)

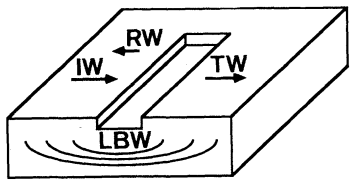

(b)

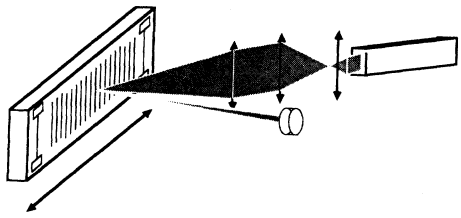

(c)

FIG. 1. (a) Schematic representation of the experimental system. Each pair of "dumbbells" on both sides of the lattice of grooves depicts a SAW transducer working either in reflection or in transmission. The propagating path is perpendicular to the array of grooves, along the large axis of the system. (b) Detail of a groove. IW stands for incident wave, RW for reflected wave, TW for transmitted wave, and LBW for leaky bulk wave. (c) Optical diffraction experimental setup which allows to obtain the local spatial structure of the proper modes. The large black arrow shows the direction of the translation imposed on the SAW device so that the laser beam may probe the SAW amplitude along it.

This array of grooves is surrounded by electromechanical transducers, laid down onto the surface of the YZ-$LiNbO_3$ crystal, performing transmission and reception of the surface acoustic waves. A transducer is generally a periodic structure of alternate electrodes (so-called interdigital structure) connected to two buses, themselves connected to the terminals of either an electric generator or an analyzer. The spectral response of the quadrupole constituted by the two transducers is centered around a frequency corresponding to the periodicity of the fingers of the transducers, with a 3 dB bandwidth depending upon the number of pairs of interdigital electrodes (typically, the frequency f is in the range 10 MHz to 2 GHz and the relative bandwidth is $\Delta f/f\sim 20\%$ for an interdigital electrode structure of three periods). These characteristics can be somewhat adjusted by an appropriate electrical surrounding.

In practice, we must allow for a number of secondary effects, among which predominate mutual reflections between transducers and between the later and the array, reflections from the edges of the crystal, transmission of bulk waves by the transducers, and the grooves which can be reinjected at the surface after reflection from the bottom of the crystal, electromagnetic radiated noise from the excited transducers. These different artifacts have been recognized[10] for a long time and can be either minimized by a suitable optimization of the structure or separated from the interesting information in the signal treatment. We will address these points, when necessary, during the exposition of the corresponding experimental results.

The SAW which has been studied is the Rayleigh wave whose characteristics for a perfect solid surface in contact with void are well known.[12] Rayleigh SAW constitutes a particular type of elastic wave in solids and can be seen as a mixture of longitudinal and transverse modes such that the condition of vanishing stress at the free solid boundary is fulfilled. They are characterized by a real wave vector in the directions parallel to the surface and a pure imaginary wave-vector component in the direction perpendicular to the surface. The SAW thus propagates along the plane and is evanescent away from the solid boundary with a typical excursion of the order of the wavelength. Rayleigh SAW's propagate with a phase velocity c_R slightly less than the phase velocity c_t of the transverse (or shear) bulk wave. The dispersion relation of the Rayleigh SAW in linear ($\omega=c_R k$) in absence of corrugation. In presence of a perturbation to the planar shape (take, for example, the case of the existence of a single groove of depth h and width w), the SAW is partially reflected with a reflection amplitude coefficient given by $\mu\approx 0.6(h/\lambda)\sin(2\pi w/\lambda)$ (Ref. 10) ($\approx 4\times 10^{-3}$ for our frequency range $f\approx 160$ MHz). Furthermore, a

fraction $p \sim \mu^2$ of the SAW energy is detrapped and converted into longitudinal and shear bulk acoustic waves.[13] Note also that the consequence of the presence of air instead of void has been well documented and is known to lead to a small well-controlled additional loss.[10]

In the general context of wave propagation in inhomogeneous systems, SAW's are particularly interesting for several reasons which we have exploited in our experiments.

(i) Rayleigh waves are well defined in frequency (for instance with a precision of 1 kHz around a main frequency of 100 MHz corresponding to a relative precision of 10^{-5}). The intensity of the wave can also be precisely monitored and kept far away from nonlinear thresholds. The wavefronts can be made planar to a good accuracy and controlled by different techniques.[10]

(ii) All the characteristics of the propagation phenomena (spectra, time response, modal structures) can be extracted experimentally. This feature is particularly interesting for testing predictions of theoretical models.

(iii) SAW propagation suffers from a relatively weak intrinsic dissipation (without speaking of the attenuation due to leakage of the guided SAW from the corrugated surface into the bulk which is discussed below).

Our experimental results are obtained as follows. We sample the frequency range of interest with a typical frequency step of 3 kHz. The temperature of the sample is regulated at ± 1 °C and the spectral response of the quadrupole is measured with a precision better than 10^{-2} dB. Because of the limited 3 dB bandwidth of the transducers which is in the range of 30 kHz around 160 MHz, the time impulse width is not vanishing but around 0.03 μs. This allows us to distinguish SAW paths with length difference of the order or larger than 100 μm.

The spatial structure of the modes is obtained from an optical diffraction setup using the Raman-Nath effect, which is presented in Fig. 1(c). A He-Ne laser beam is focused on the sample and the diffraction pattern is detected with a photodiode. The Raman-Nath effect can be viewed as the diffraction of light by an acoustic wave of finite extent and therefore of indeterminate wave vector. In this regime which is different from the usual bulk Bragg diffraction, the laser beam is split, after interacting with the acoustic wave, into several beams of different orders of diffraction each corresponding to the absorption or emission of a different number of phonons.

In order to improve the signal-to-noise ratio of the experiments, we used a lock-in amplification in the detection of a 1 kHz amplitude modulated SAW. The wave amplitude was then drawn on an X-Y chart recorder as the sample was moved.

III. THE SPECTRUM

Figure 2 gives the value of the SAW transmission coefficient of the system as a function of the frequency. The bell-like global shape corresponds to the transducers filtering. Two families of stop bands decorate this large-scale structure. The first family, shown in Fig. 2 by the large arrows is made of equidistant peaks with period $\Delta f_P = 4.85 \pm 0.02$ Mhz. This corresponds to a reciprocal wave vector $\Delta k_P = 2\pi \Delta f_P / c$ which is also related to the

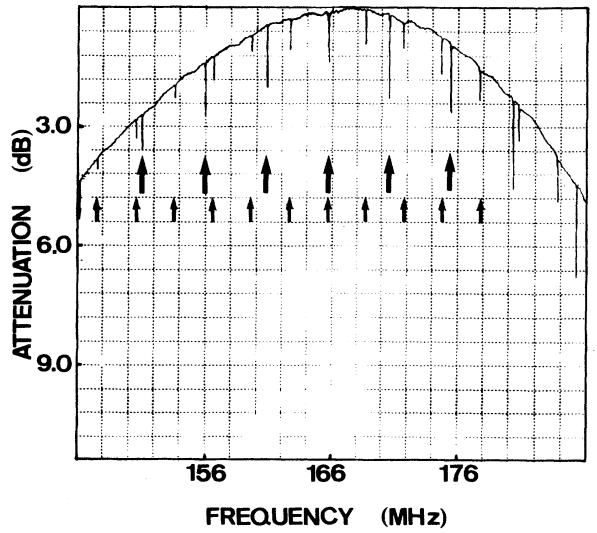

FIG. 2. Value of the SAW energy-transmission coefficient of the system as a function of frequency. The large (small) arrows show the stop bands of the periodic Q (P) subsystem of period $Pd_{\min}$ ($Qd_{\min}$). The large-scale bell-like shape of the curve corresponds to the passing band of the transducers.

periodicity $Pd_{\min}$ of the Q sublattice by $\Delta k_P = \pi / Pd_{\min}$. This yields an experimental determination $Pd_{\min} = 357.5 \pm 1.5$ μm which compares very well with the exact value 358.5 μm. We have used the value $c = 3468$ m/s measured in the impulse response (see Sec. V). For the other family shown in Fig. 2 with small arrows, the analysis is similar and we measure $\Delta f_q = 3 \pm 0.01$ Mhz leading to $Qd_{\min} = 578 \pm 2$ μm which compares very well with the exact value 576 μm. The experimental value for P/Q is thus 0.6185 ± 0.0005 and approaches very well the exact value $89/144 = 0.6181$.

This spectrum has been predicted in Ref. 1 on the basis of a transfer-matrix formulation[14] which is reduced to the study of the dynamics of the phase shift between forward and backward waves; this leads to the iteration of a nonautonomous mapping on the circle.[1] A continuous spectrum of passing bands separated by δ-like gaps is predicted in the limit of quasiperiodicity (i.e., $P = F_j$, $Q = F_{j+1}$, with $j \to +\infty$) and in the zero reflection coefficient per groove limit ($\mu \to 0$). In these limits, the set of gaps is given by the Fourier transform of $n(x)$ which is simply the superposition of the Fourier transforms of the two subsystems of period P and Q, as verified on Fig. 2. The finite value of the reflection coefficient enlarges the gaps and makes them observable. The finite size N of the sample introduces in addition a rounding of the gaps over a frequency range of the order of N^{-1}.

Note that Fig. 2 contains other information specific to this experimental SAW system. Indeed, the peaks on Fig. 2 have not all the same size and one observes a systematic rise in the amplitude of the inverted peaks of the stop bands as the SAW frequency increases. This can be related to the variation of the single groove reflection coefficient with the frequency known from perturbation theory[13] as

$$\mu = 0.6(h/\lambda)\sin(2\pi w/\lambda)$$
$$\sim hw/\lambda^2 \text{ for our range of } \lambda . \quad (2)$$

The typical value of μ at $f \approx 160$ Mhz is $\mu \approx 4.5\times10^{-3}$. Note that one expects a transmission coefficient of the form $T = T_0\exp(-\alpha\mu L)$ which decreases as μ increases or λ decreases. This explains the trend observed in Fig. 2 showing an increase of the peaks at larger frequencies.

This quasiperiodic system presents also a particular feature on its spectrum, namely a pair of very close gaps shown in Fig. 3 with a narrow passing band between them, which has been termed the "fundamental pass band" in Ref. 1. Our observation in Fig. 3 is well in agreement with the prediction of Ref. 1 concerning this band in spite of the presence of several additional phenomena, such as the wave attenuation, which are not taken into account in the model. In the limit of a small reflection coefficient μ, it has been shown that the frequencies corresponding to the dominant stop bands of the system are given exactly by

$$n(f) = \sum_m \delta(2kd_{\min} - mP) + \sum_n \delta(2kd_{\min} - nQ) \quad (3)$$

which is the simple superposition of the two patterns of stop bands, one for each periodic sublattice. Those special frequencies such that there exist two integers m and n such that $2kd_{\min} = mP$ is very close to nQ correspond to the "fundamental passing bands." In fact, there existence is related to specific diophantine properties of Fibonacci numbers[15] which determine the best values for m and n such that mP and nQ are as close as possible,

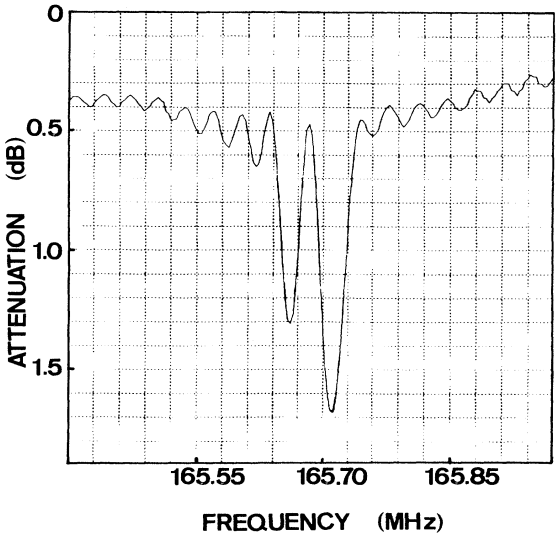

FIG. 3. Detail of the spectrum obtained in transmission showing a pair of very close gaps with a narrow passing band between them, which has been termed the "fundamental pass band" in Ref. 1. Note the dissymmetry of the two inverted peaks which amplitudes are related to the number of grooves ($P = 89$ and $Q = 144$) pertaining to each periodic subsystem. The deeper peak corresponds to the periodic P subsystem which has the largest number ($Q = 144$) of grooves and the other peak corresponds to the periodic Q subsystem having $P = 89$ grooves.

namely $F_{n+1}F_{n-2} - F_nF_{n-1} = (-1)^n$, known as the Cassini identity. Indeed, let us note

$$k = \pi\nu/L \quad (4)$$

is a given reciprocal-lattice wave vector, with ν being an integer running from 1 to PQ. The fundamental pass band corresponds to the ν interval $[F_jF_{j-1}, F_{j+1}F_{j-2}]$. With $j = 10$ as in our experimental system, this leads to ν in the interval [4895,4896]. This corresponds to a surface acoustic wavelength $\lambda = L/\nu$ in the interval [20.941 μm, 20.945 μm] and to a frequency width given by $\Delta f/f = 2\times10^{-4}$.

Experimentally, we measure the center of the band at $f = 165.68\pm0.02$ MHz corresponding to $\lambda = 20.93\pm0.01$ μm in excellent agreement with the prediction. The width of the band can be estimated as a fraction of the distance between the two inverted peaks and is found of the right order of magnitude compared to the expected value of about 3×10^{-2} MHz, taking account of the rounding bands induced by the finite size of the system. The rounding of the bands can be measured by the parameter $\Delta f/f$, ratio of the frequency rounding over the frequency f. It is related to the finiteness of the system by $\Delta f/f \sim \lambda/2L \approx 2\times10^{-4}$ which corresponds nicely to the measured value.

Let us finally discuss the expected values of the quality factor Θ in the vicinity of this passing band and compare it with the prediction of Ref. 1. By definition, $\Theta = f/\Delta f$, where Δf is the frequency rounding. Taking the theoretical value $\Delta f \approx 3.5\times10^{-2}$ MHz and $f = 165.7$ MHz, we have $\Theta \approx 4730$.

On the other hand, $f/2\pi\Theta$ is equal by definition to the ratio (lost energy flux)/(stored energy) $= c(1-R)/L$ since $1-R$ is the loss for the reflection (assuming an infinite system and therefore a vanishing transmission). This implies that $\Theta = fL/4\pi(1-R)c$. In our case, $1-R = I(L)/I_0$ (neglecting the loss phenomena) which is found to be approximately equal to 6.8×10^{-2} (Ref. 1) [see Eq. (7) in Sec. IV where $I(L)/I_0$ is calculated explicitly]. This gives $\Theta \sim 5000$ compatible with the preceding estimation.

Peyraud and Coste have estimated theoretically in Ref. 1 that Θ obeys the following asymptotic equation:

$$\Theta = \mu^{1/2}L^{1/4}\exp(\alpha\mu L^{1/2}) . \quad (5)$$

The $L^{1/2}$ dependence in the exponential of Eq. (5) stems from the fact that the number $N = P + Q$ of scatterers grows like $L^{1/2}$ for large L. Taking $\Theta \approx 5000$, we obtain the value $\alpha \approx 16$ for the coefficient in the exponential of Eq. (5). Equation (5) shows that Θ increases as the exponential of the square root of the system size in this quasiperiodic system.

Let us compare this result to the case of a simple periodic system of period a inside of which one introduces a transducer so as to launch a SAW inside it. Using the previously discussed expression for $\Theta = fL/4\pi(1-R)c$, we use $1-R \approx e^{-L/\xi}$, with $\xi = a/\mu$ at the Bragg condition, and replace L by ξ since it is the effective length over which the SAW can penetrate inside the periodic system. This yields finally

$\Theta=\pi/2(1-R)\mu\sim(\pi/2\mu)\exp(\mu L/a)$ which shows that Θ increases exponentially with L and is therefore much larger than that of the quasiperiodic system. In this case, the number of scatterers grows like L and thus the frequency resolution is much better.

In such passing bands, Peyraud and Coste have predicted the existence of quasilocalized modes. This is related to the fact that one can expect special behaviors near a gap and thus, particularly so, between two gaps in such close proximity.

IV. THE SPATIAL STRUCTURE OF THE FUNDAMENTAL MODE

In the fundamental passing band seen in Fig. 3, a special quasilocalized proper mode was predicted to appear.[1] The spatial structure of this quasilocalized mode obtained with the optical diffraction technique described in Ref. 16 is reported in Fig. 4 for the case when the SAW is incident from one side (condition of "nonzero flux"). One observes that the wave amplitude decreases at first rapidly with distance along the system before increasing again due to the existence of the quasilocalized mode. Note also the short scale complex pattern which probes each single groove diffraction pattern as the sample is moved in front of the focused laser beam spot.

In Figs. 5 and 6 are reported the spatial structure of the SAW amplitude for the case when two incident waves from the left and from the right are impinging on the system (condition of "zero energy flux"). Figure 5 is obtained from Fig. 6 by defocusing the laser beam illuminating the sample so that most of the small scale

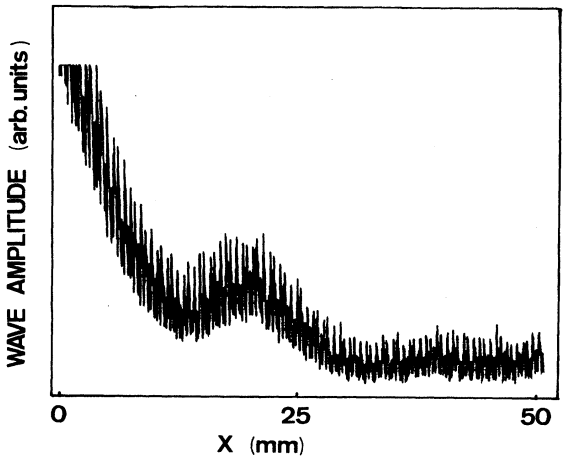

FIG. 4. Spatial structure of the fundamental quasilocalized mode obtained with the optical diffraction technique shown in Fig. 1(c) and described in Ref. 16. The SAW is incident from the left-hand side ("nonzero flux" condition). The amplitude of the SAW is detected by a photoelectric cell and drawn directly on an X-Y chart recorder without any signal processing. One observes that the wave amplitude decreases at first rapidly with distance along the system before increasing again due to the existence of the quasilocalized mode. Note the short scale complex pattern which probes each single groove diffraction pattern as the sample is moved in front of the focused laser-beam spot.

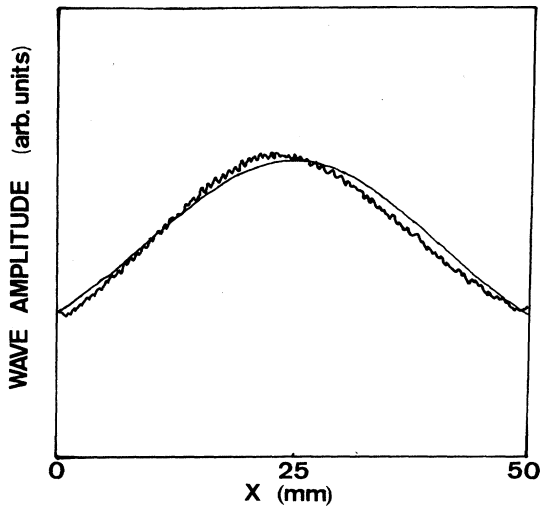

FIG. 5. Spatial structure of the fundamental quasilocalized mode obtained with two SAW incident from the left and from the right onto the system (condition of "zero energy flux"). This averaged pattern is obtained by defocusing the laser beam illuminating the sample. The smooth curve is obtained numerically from the theory of Ref. 1.

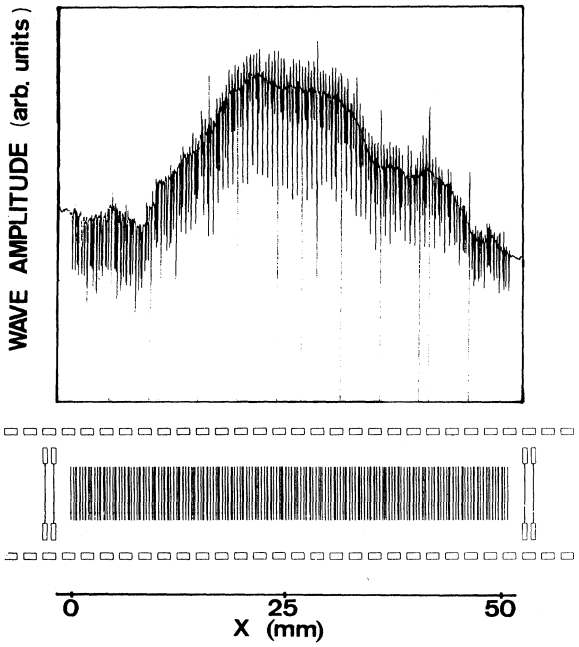

FIG. 6. Same as Fig. 5 but with a spatial resolution of the optical probe of the order of 50 μm which is obtained by focusing the laser-beam spot. This resolution must be compared with the average groove spacing $a=221$ μm. The signal-to-noise ratio is increased by the use of a lock-in amplification. The observed slight dissymmetry of the mode structure is attributed to an imperfect "zero flux" condition. As in Fig. 4, the belllike mode shape is decorated by the diffraction pattern of the grooves.

structure is smoothed out. In Fig. 5, the smooth curve has been obtained numerically from the analysis of Peyraud and Coste in the same condition of zero energy flux. The agreement between the two curves is striking. However, Fig. 6 exhibits a more complex structure at smaller scales obtained with a more precise experiment with a spatial resolution of the order of 50 μm. The spiky structure observed at scales of the order of the average groove separation can be attributed to effects working at the scale of each single groove. At this scale, the SAW and bulk wave amplitude are complex and are sensitive to the nonpointlike structure of the grooves. A precise study of the local SAW amplitude at these scales would be certainly worthwhile in order to understand the influence of the local features of the SAW pattern on the large scale structure stemming from multiple interference effects. Note also the existence of very deep inverted peaks which corresponds to pairs of grooves having a very small separation. This observation points at the importance of nontrivial interactions between neighboring grooves. We hope to return to these problems in the future.

Figure 6 shows also the existence of modulations at scales intermediate between the groove and system sizes. This is not predicted from the analysis of Ref. 1, valid under a coarse-graining approximation which relies on the existence of a slow variable in the wave propagation. The validity of this coarse-grained approach relies on the condition $\mu \gg Q^{-1}$, implying that finite-size effects are small. With our system $\mu \approx 0.5$ % and $Q^{-1} \approx 0.7\%$ and this condition is not strictly fulfilled. This may be a partial explanation for the discrepancy between Fig. 5 and Fig. 6. Also, a coarse-grained treatment is not precise enough for predicting fine details. A reasonable theoretical description of the mode profile should involve a direct transfer-matrix formalism and possibly use transfer matrices taking account explicitly of the finite size of the grooves and of the interaction between them.

Around its maximum, the amplitude profile of the fundamental mode has the following asymptotic analytical form:[1]

$$I(x)=I_0\exp[-F_j\mu(2\pi x/L)^2/2\sqrt{t}\,]\,, \tag{6}$$

where F_j is the jth Fibonacci number related to the size L of the system by $L=F_jF_{j+1}d_{\min}$ showing that in the limit of large j, $F_j \sim L^{1/2}$. μ is the amplitude reflection coefficient per groove given by Eq. (2) and t the inverse golden mean. Thus, for large j, $I(x) \sim \exp[-\alpha\mu(x/L^{3/4})^2]$ where α is a numerical factor. With $j=10$, $F_{10}=89$, $\mu \approx 4.8\times 10^{-3}$ at the frequency $f=165.7$ MHz, Eq. (6) gives

$$I(x)=I_0\exp[-10.75(x/L)^2]\,. \tag{7}$$

The half-width of the mode at $1/e$ is therefore $x/l \approx 0.3$ which explains its rather smooth peaked structure. If we could have made a system with a higher j, the localized structure of the mode would have been much clearer since F_j increases exponentially with j (see, for example, Fig. 7 of Ref. 1 obtained for $j=12$ and $j=15$). However, we were limited by experimental constraints on the minimum size of the grooves and the maximum size of the system.

Note that this mode is special since its norm diverges as L increases according to[1]

$$\int_{-L/2}^{L/2} I(x)dx \sim L^{3/4} \tag{8}$$

and is therefore not really localized in the usual sense.[17] Furthermore, defining the "sojourn time" T_Λ in a box Λ as being proportional to the ratio (energy stored in Λ)/(energy flux), one finds[1] that $T_\Lambda \to +\infty$ when $L \to +\infty$. This special mode has an infinite norm (and therefore would qualify as being extended in this sense) and in the same time an infinite sojourn time (and would correspond to a localized mode in this sense). It is reminiscent of proper modes which occur for some other quasiperiodic systems[2] and which are associated to a singular continuous spectrum.[17]

To end this section, we would like to stress the physical origin of this fundamental mode and argue that it is related to the general existence of localized modes in other quasiperiodic or random systems. This will show that this most simple system (1) is particularly well suited to present pedagogically the origin of mode localization in inhomogeneous structures.

Heuristically, the nature of this mode can be understood as follows. Note first that the quasiperiodic system possesses a center of symmetry at $x=L/2$. The system can therefore be viewed as constituted by two equivalent half-systems each being the mirror image of the other and placed side by side. At frequencies inside the "fundamental passing band" of the whole system, each identical half-system presents a stopping band. This means that any solution of these half-systems at these frequencies should either increase or decrease exponentially with distance. Physically, the solution decreasing exponentially inside each half-system is selected. But, due to their setting side by side and from the existence of the center of symmetry, the whole system develops proper modes which can then be interpreted as resulting from a coherent tunneling through each half-stopping system. We can now understand that the center of symmetry insures the matching of the solution decaying to the left in the first half-system with the solution decaying to the right in the second half-system in the precise frequency range corresponding to the fundamental pass band. This explains the bell-like shape of the mode depicted in Figs. 4–6. This line of reasoning is reminiscent of the general Borland's type argument for the construction of localized states in one-dimensional (1D) random systems.[18]

V. ANALYSIS OF THE IMPULSE RESPONSE

The information in the time domain is in principle equivalent to that obtained from the spectrum discussed in Sec. III since it is obtained from it by a simple Fourier transform. We have verified this point in our experiments: the impulse response obtained experimentally is indistinguishable from the Fourier transform of the experimentally determined frequency spectrum.

However, it gives a nice complementary picture of the SAW propagation which may be in some cases more in-

tuitive. A number of undesirable effects are well isolated in the time domain and can even be filtered out. For instance, this happens for the spurious reflections between transducers. Also, certain features are much clearer in the time domain. It can be very useful for locating the position of the scatterers. This study may also serve as a paradigm of acoustic wave probing techniques which are essentially implemented in the impulse time domain,[19] as for example, in geological survey of natural resources.

A. Time response under reflection

Figures 7 and 8 show the impulse response under reflection of the quasiperiodic system. Note that the succession of pulses reproduces the quasiperiodicity of the system in the time domain. Since the average distance between the grooves is 221 μm, each individual groove gives a distinctive and measurable signal, except in some cases where two grooves happen to be positioned within a distance smaller than the pulse duration which corresponds to a spatial extension of the order of 100 μm. Indeed, with a 3 dB bandwidth of 32.5 MHz due to the transfer function of the transducers, we expect a temporal resolution time of 0.03 μs which corresponds to a flight distance ~ 100 μm. In Fig. 7, we identify the pulses corresponding to a simple reflection over the successive grooves of the quasiperiodic system, which can be represented as follows for the few first grooves (in units of $d_{\min}=4$ μm):

Q subsystem	0	89	178	267	356	445	534	623	712	$\cdots$	Period $Pd_{\min}=89d_{\min}$
P subsystem		144		288	432		576		720	$\cdots$	Period $Qd_{\min}=144d_{\min}$.

"0" corresponds to the first groove, "89" to the second groove of the period P placed at a distance equal to $89d_{\min}$, etc. In this series, each groove gives its distinctive pulse except for the two grooves at 712 and 720 which are separated by a distance $(720-712)d_{\min}=32$ μm. The effective length covered by the pulse in reflection is twice this distance (direct and return) and is thus of the order of the pulse width.

The intensity of the pulses which are reflected on the first grooves gives a measure of the reflection coefficient $10\log_{10}\mu^2=-46.25\pm0.1$ dB which yields $\mu=4.8\pm0.1\times10^{-3}$ which is in good agreement with the theoretical value $\mu=0.6(h/\lambda)\sin(2\pi w/\lambda)=4.6\times10^{-3}$ around the central frequency 160 MHz. In Fig. 9, one can identify two regimes: from the time $t_1\approx1.445$ μs (arrow A) to $T_2\approx31.005$ μs (arrow B), we measure essentially the sin-

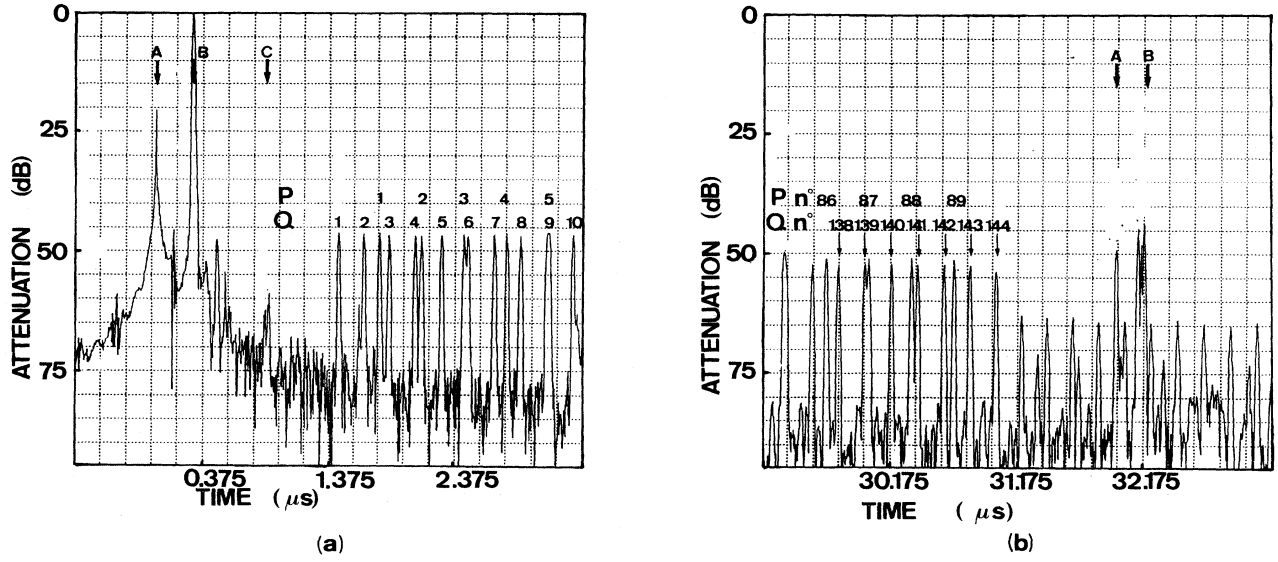

FIG. 7. Details of the time impulse response under reflection shown on Fig. 9. The SAW is launched from one transducer ($T1$) at the left of the system and is received by a second transducer ($T2$) placed in between the transducer ($T1$) and the system. (a) Short times. The arrow A corresponds to the direct electromagnetic propagation from $T1$ to $T2$ and is taken as the origin of time for the SAW propagation. The reference peak B corresponds to the direct surface acoustic wave propagation from $T1$ to $T2$. The peak C corresponds to the SAW triple reflection on the transducers $T1$ and $T2$. Note that one can identify the partial pulse reflections on each single groove. This is exemplified by the two sequences denoted P and Q which correspond exactly to the structure of the system. Each number denotes the groove belonging to one of the two systems on which the pulse has undergone reflection. (b) Long times. This figure shows the last single reflections on each individual groove and the transition to a triple reflection regime at long times. Peak A corresponds to the SAW reflection upon the up step placed at the right of the system of grooves. Peak B corresponds to the reflection on the grounded transducer placed at the right of the system.

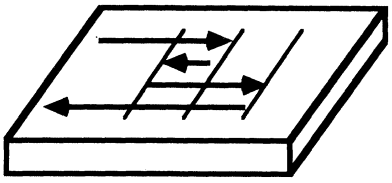

FIG. 8. A typical path of the SAW in reflection which exhibits three successive reflections on three grooves.

gle reflections on the successive grooves. The pulses received on the transducer at times larger than t_2 corresponds to triple reflections of the form shown in Fig. 8. The measured time for covering the distance $2L=102\,528\ \mu$m is $t_2-t_1=29.56\pm0.02\ \mu$s. This yields a measured SAW group velocity $c=3468\pm2$ m/s. This is in reasonable agreement with the velocity $c=3485(\pm5)$ m/s known for a (YZ-$LiNbO_3$) smooth substrate at room temperature (the relative velocity variation with temperature is of the order of 10^{-4}/°C).

The measure of the slope of the logarithm of the individual pulses intensity versus time yields the attenuation. We measure a global attenuation of 5.7 ± 0.6 dB for a propagation over a time of 29.56 μs taken by the wave for a round trip ("*aller-retour*") over the array. This corresponds to a characteristic attenuation time $l_a/c=21.3\pm0.5\ \mu$s and $l_a=75\,000\pm2000\ \mu$m.

We can distinguish between the contribution of intrinsic dissipation and coherent losses (surface to bulk detrapping).[10,13] With the known formula[10] $P_{\rm ID}(\mathrm{dB}/\mu s)=0.19f+0.88f^2$ for the intrinsic dissipation per μs (where f is given in GHz), we obtain $P_{\rm ID}=1.6$ dB for the

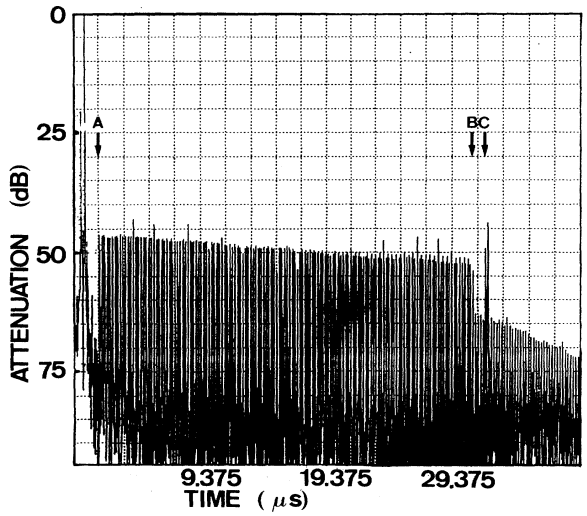

FIG. 9. Large-scale time impulse response under reflection on the quasiperiodic system. A (response B) denotes the reception of the pulse after *single* reflection upon the first (last) groove of the system. After B, pulse trajectories having suffered triple reflection as shown in Fig. 8 can be observed. The arrow C shows some spurious peaks corresponding to the reflection on the grounded transducers on the other side of the system.

aller-retour over the system and by difference we can estimate the total power loss due to SAW leakage over an *aller-retour* $P_{\rm coh}=4.1$ dB with 10% accuracy. Then, the coherent loss for a single passage of the SAW over one groove is $P_{\rm coh/groove}=0.0088$ dB and must be compared to the amount of reflected energy per groove: $\mu^2=(4.8\times10^{-3})^2=2.3\times10^{-5}$. This leads to $P_{\rm coh/groove}\sim90\mu^2$. The factor 90 is much greater than expected usually[13] (a factor of order 20–30 is often reported).

Using the optical diffraction technique described in Sec. II, we have probed the SAW intensity profile in the direction transverse to the lattice axis. This has permitted us to verify that the SAW propagation was correctly directed along the axis of the lattice. Therefore, the large measured loss factor cannot be explained by a "beam walkoff" effect, but rather seems characteristic of the grooves which have been used.

Let us now analyze in details the second regime at times larger than t_2 corresponding to the triple reflections seen in Fig. 7(b). We identify two families of peaks. The first one is constituted of equidistant peaks separated by a time interval $\Delta t_P=0.204\pm0.005\ \mu$s corresponding to the propagation (direct and return) over a distance $c\Delta t_P/2=354\pm3\ \mu$m in good agreement with the period $Pd_{\rm min}=356\ \mu$m. The second one is constituted of equidistant peaks separated by a time interval $\Delta t_Q=0.333\pm0.005\ \mu$s corresponding to the propagation (direct and return) over a distance $c\Delta t_Q/2=577\pm2\ \mu$m in good agreement with the period $Qd_{\rm min}=576\ \mu$m.

The two periodic subsystems reappear in the triple reflection since only the SAW trajectories with a triple reflection on a same periodic sublattice and corresponding to the same time arrival are sufficiently numerous to give an important signal. This is due to the fact that a single triple reflection signal is $10\log_{10}\mu^4\approx-47$ dB below a single simple reflection signal. Thus, many SAW trajectories must add coherently to increase the triple reflection signal which are measured in Fig. 7(b) at only 8–10 dB below the simple reflection signals.

Let us first analyze this problem quantitatively on the subsystem of period P which possesses $Q=144$ grooves. Consider a particular triple reflection SAW trajectory and let us note $1<n_1\le Q$, the number of the groove on which the first reflection occurs, $1\le n_2<n_1$, the number of the groove on which the second reflection occurs and $n_2<n_3\le Q$, the number of the groove on which the third reflection occurs. Then, the time of arrival of the SAW trajectory is

$$t_{\rm SAW}=\tau[n_1+(n_1-n_2)+(n_3-n_2)+n_3]$$
$$=2\tau[n_1-n_2+n_3]\ , \qquad (9)$$

where τ is the time taken by the SAW for propagating over one period $Qd_{\rm min}$. Our problem is now to determine the number of trajectories, i.e., triplets (n_1,n_2,n_3) such that

$$n_1-n_2+n_3=t_{\rm SAW}/2\tau \qquad (10)$$

with $t_{\rm SAW}$ fixed. Let us note $n=n_1-n_2$. Then, the con-

dition (10) reads

$$n+n_3=t_{\mathrm{SAW}}/2\tau\ . \tag{11}$$

The number of couples (n,n_3) with $n,n_3\geq 1$ which obey Eq. (11) is equal to the number of points given by $(t_{\mathrm{SAW}}/2\tau)-1$ in the plane (n,n_3) which are positioned on the line whose equation is (11). For each such couple, i.e., at n fixed, there are $Q-n$ couples (n_1,n_2) such that $n=n_1-n_2$. Thus, the total number of triplets (n_1,n_2,n_3) verifying Eq. (10) is given by

$$\begin{aligned} N(t_{\mathrm{SAW}}) &= \sum_{n=1}^{(t_{\mathrm{SAW}}/2t)-1} (Q-n) \\ &= Q[(t_{\mathrm{SAW}}/2\tau)-1] \\ &\quad -(t_{\mathrm{SAW}}/4\tau)[(t_{\mathrm{SAW}}/2\tau)+1]\ . \end{aligned} \tag{12}$$

Let us now predict the intensity of the first triple reflection. This corresponds to $(t_{\mathrm{SAW}}/2\tau)=Q$ and $N(t_{\mathrm{SAW}})=0.5Q^2-1.5Q=10\,152$. Thus, about 10^4 different SAW trajectories with triple reflections add coherently and build the measured signal. Its intensity is thus given by

$$\begin{aligned} I_{\mathrm{triple}}(t_{\mathrm{SAW}}) &= 10\log_{10}[N^2(t_{\mathrm{SAW}})\mu^6] \\ &= -60.7\ \mathrm{dB}\ . \end{aligned} \tag{13}$$

Experimentally, we measure in Fig. 7(b) a signal -66 ± 1 dB below the reference. The difference can be understood by taking account of the attenuation. Indeed, for a travel time of $2\tau Q=29.56\ \mu$s, one expects an attenuation of $10\log_{10}\exp(-2\tau Qc/l_a)=-6$ dB. We thus obtain a remarkable agreement by adding the theoretical value $I_{\mathrm{triple}}(t_{\mathrm{SAW}})=-60.7$ dB and the attenuation of -6 dB. It is remarkable that we are able to identify experimentally the contribution of as many as 10^4 SAW triple reflection trajectories. This reasoning can also explain the dependence of the pulse intensity as a function of time, by replacing the expression (12) for $N(t_{\mathrm{SAW}})$ in Eq. (13). This leads to

$$I_{\mathrm{triple}}(t_{\mathrm{SAW}})\approx I_{\mathrm{triple}}(t_{\mathrm{SAW}}=2\tau Q)-0.2056(t_{\mathrm{SAW}}/2\tau)^2\ . \tag{14}$$

We expect, therefore, a decrease of -38 dB over a time interval of 40 μs which must be compared to the measured -43 dB. Again the difference stems from the wave attenuation, which for 40 μs is of the order of 8 dB.

B. Time impulse response under transmission

Figures 10 and 11 show the impulse response under transmission of the quasiperiodic system. The large peak of intensity of 0 dB (which serves as a reference) corresponds to the direct propagation over the whole length of the system. The latter peaks correspond to double reflections of the type shown in Fig. 12.

As for the impulse response in reflection, we can understand the intensity of the pulse by summing the contribution of the different double reflection SAW trajectories arriving on the transducer at the same time. We

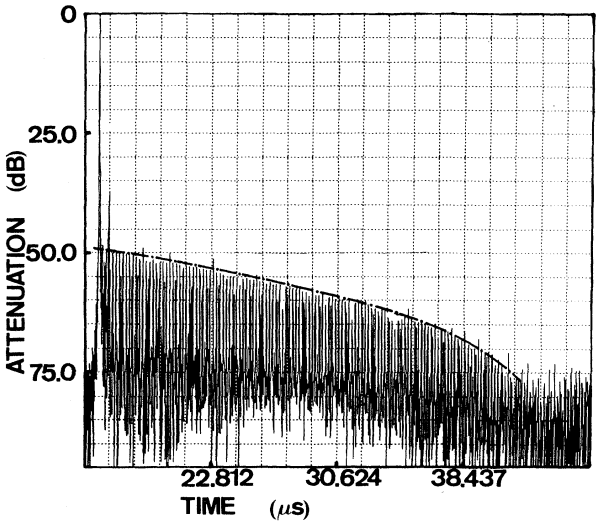

FIG. 10. Large-scale impulse response under transmission of the quasiperiodic system as a function of time. The largest peak at 0 dB corresponds to the direct transit over the sample, from the launching transducer on its left to the receiving transducer on its right. The dotted-dashed line is the theoretical prediction of the pulse intensity in transmission as a function of time, discussed in the text. It takes account of the number of different double reflection SAW trajectories arriving on the transducer at the same time as a function of time, including the attenuation.

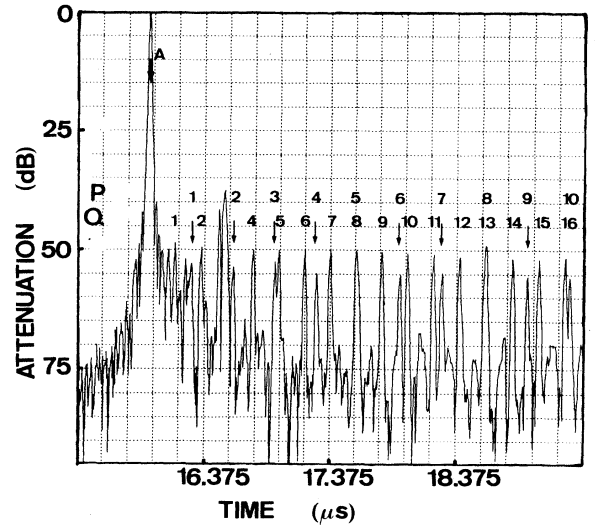

FIG. 11. Details of the time impulse response under transmission shown in Fig. 10. As in Fig. 7, one can identify the spatial pulse reflections on each groove. The difference with Fig. 7 is that each individual pulse response corresponds to a double reflection path as depicted in Fig. 12. This accounts for the observation of two pulse subsystems corresponding to the two periodic subsystems of Q and P grooves etched on the sample. Note that, as discussed in the text, crossed reflections on a pair of grooves, one of which belongs to the P subsystem and the other one to the Q subsystem, are too scarce in order to build a strong enough signal which can be sorted out of the noise.

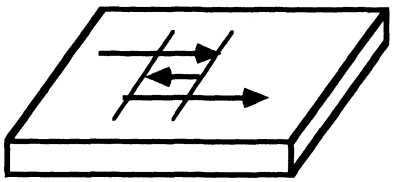

FIG. 12. A typical path taken by the SAW in transmission exhibiting two successive reflections on two grooves.

obtain, for the first peaks

$$I_P = 10\log_{10}(Q^2\mu^4) = -50.6 \text{ dB} , \quad (15a)$$

$$I_Q = 10\log_{10}(P^2\mu^4) = -55 \text{ dB} , \quad (15b)$$

which are in very good agreement with the measurements. We also obtain an estimation of the golden mean by

$$P/Q = 10^{(I_Q - I_P)/20} = 0.60 \pm 0.02 . \quad (16)$$

The concave shape of the envelop of the pulse intensity as a function of time can be explained by taking account of the number of different double reflection SAW trajectories arriving on the transducer at the same time as a function of time:

$$I_P(t_{\text{SAW}}) = 20\log_{10}(1 - n/Q) , \quad (17)$$

where n is the distance between the two reflections. In the time domain, with a time interval of $2Pd_{\min}/c$ between successive peaks, this gives

$$I_P(t_{\text{SAW}}) = 20\log_{10}(1 - t_{\text{SAW}}/29.56) \quad (18)$$

with t_{SAW} expressed in μs. As shown in Fig. 10, Eq. (18) gives a curve following very well the envelop of the pulses when including the attenuation of the order of -4.5 dB at time $t_{\text{SAW}} \approx 22$ μs.

VI. CONCLUSION

We have presented experimental results and their interpretation on the propagation of surface acoustic waves on a particular one-dimensional quasiperiodically corrugated solid surface. It has been constructed by a simple superposition of two periodic lattices of periods P and Q such that P/Q approaches a particular irrational number, the golden mean. This problem has previously been studied theoretically in the limit of vanishing corrugation in Ref. 1. We have reported precise results about the transmission frequency dependence, the temporal impulse response both in reflection and transmission and the spatial structure of the proper modes. The theoretical predictions were well observed experimentally. Note however that the validity of the coarse-grained approach developed in Ref. 1 relies on the condition $\mu \gg Q^{-1}$, implying that finite-size effects are small. With our system ($\mu \approx 0.5\%$ and $Q^{-1} \approx 0.7\%$), this condition is not strictly fulfilled. Our results can thus be taken as a clue that the theoretical results derived in Ref. 1 are robust with respect to the condition $\mu \gg Q^{-1}$. It would be interesting to go beyond the coarse-grained treatment of Ref. 1 to demonstrate this fact.

Let us now discuss some open problems. A first one concerns a proper description of the surface to bulk wave conversion by a groove in presence of all the other grooves. Spectacular effects concerning the vanishing of this leakage have been observed for periodic systems and in another quasiperiodic system studied in Ref. 20. They seem to involve coherent destructive interferences at infinity between all the partial wavelengths emitted in the bulk by the different grooves. In terms of a local SAW description, this implies the existence of long range correlations between the SAW propagation in groove arrays. These correlations are difficult to describe theoretically, for example within a transfer-matrix formalism.[14] For this problem, our quasiperiodic system could provide interesting information due to the rather large value of the average distance between grooves and the existence of a large set of different distances between nearby grooves. In principle, this could allow the observation of the effect of groove coupling as a function of their distance. We hope to come back to this problem in the future.

A second open problem concerns the fine scale structure of the fundamental proper mode observed in Figs. 4–6. Preliminary results, with a finer optical resolution than the best used in the experiments reported here, point at the role of step discontinuities which should be considered separately and not in pairs (each pair "down-up" constituting a groove). We also intend to come back more carefully on this point.

ACKNOWLEDGMENTS

We are grateful to J. Peyraud and J. Coste for stimulating discussions and for providing the numerical curve in Fig. 5. We thank J. F. Gelly and C. Maerfeld for their kind welcome in the DTAS Department of Thomson-Sintra at Sophia-Antipolis where the acoustic experiments have been carried out. The financial support from Direction des Recherches et Etudes Techniques (DRET) under Contract No. 86/177 for the research program "Propagation acoustique en milieux aléatoires" is gratefully acknowledged. Laboratoire de Physique de la Matière Condensée is Unité Associée No. 190 du Centre National de la Recherche Scientifique.

*Present address: Spectec S.A., 14 Avenue Saint Augustin, 06300 Nice, France.

[1] J. Peyraud and J. Coste, Phys. Rev. B **37**, 3979 (1988).
[2] See, for example, J. B. Sokoloff, Phys. Rep. **126**, 189 (1985), and references therein.
[3] R. Merlin, K. Bajema, R. Clarke, F. Y. Juang, and P. K. Bhattacharya, Phys. Rev. Lett. **55**, 1768 (1985).
[4] R. Riklund and M. Severin, J. Phys. C **21**, 3217 (1988).
[5] F. Laruelle and B. Etienne, Phys. Rev. B **37**, 4816 (1988).
[6] P. Hawrylak, G. Eliasson, and J. J. Quinn, Phys. Rev. B **36**, 650

(1987).

[7]M. Kohmoto, B. Sutherland, and K. Iguchi, Phys. Rev. Lett. **58**, 2436 (1987).

[8]C. Schwartz, Appl. Opt. **27**, 1232 (1988).

[9]D. Shechtman, I. Blech, D. Gratias, and J. W. Cahn, Phys. Rev. Lett. **53**, 1951 (1984).

[10]E. A. Ash and E. G. S. Paige, *Rayleigh-Wave Theory and Application* (Springer-Verlag, Berlin, 1985); A. A. Oliner, *Acoustic Surface Waves,* Vol. 24 of *Topics in Applied Physics* (Springer-Verlag, Berlin, 1978).

[11]J. R. Chamuel and G. H. Brooke, J. Acoust. Soc. Am. **84**, 1363 (1988).

[12]L. Landau and E. Lifchitz, *Théorie de l'Élasticité* (Mir, Moscow, 1967).

[13]N. E. Glass and A. A. Maradudin, J. Appl. Phys. **54**, 796 (1983); E. L. Cambiaggio and F. C. Cuozzo, IEEE Trans. Son. Ultrason. **SU-26**, 340 (1979); A. Ronnekleiv and J. Souquet, Ultrasonics Symp. Proc. IEEE Cat. 75, CHO 994-4SU (1975); J. Appl. Phys. **47**, 4422 (1976); J. Menngailis, R. C. Williamson, J. Holtham, and R. C. M. Li, Wave Electron. 2, 177 (1976); E. Baron, Thèse de Troisième Cycle, Paris 7 (1986); E. Baron, M. de Billy, and G. Quentin, Rev. Phys. Appl. **20**, 369 (1985).

[14]D. Sornette, L. Macon, and J. Coste, J. Phys. (Paris) **49**, 1683 (1988).

[15]W. Narkiewicz and S. Kanemitsu, *Number Theory* (World Scientific, Singapore, 1983), Chap. 8.

[16]J. P. Monchalin, IEEE Trans. Ultrason. Ferr. Freq. Control **UFFC-33**, 485 (1986).

[17]See, for examples B. Souillard, in *Chance and Matter,* in *Proceedings of the Les Houches Summer School, Session XLVI, 1986,* edited by J. Souletie, J. Vannimenus, and R. Stora (North-Holland, Amsterdam, 1987), and references therein.

[18]An extension of the Furstenberg theorem for a product of random matrices states that "for almost every realization of the potential and for almost every frequencies, the solutions of the propagation equation are either exponentially increasing or decreasing for $x \to +\infty$ and exponentially increasing or decreasing for $x \to -\infty$." Since physical states cannot increase exponentially, Borland concluded that the only physical states occur for those frequencies for which two decreasing solutions for $x \to +\infty$ and for $x \to -\infty$ correspond to the same value at site say 0 and 1, i.e., we have matched the solution decaying on the left with the solution decaying on the right. Borland's argument is essentially correct if one allows change in the value of the scattering potential (grooves) on two sites (see Ref. 17 for details).

[19]P. Sheng, Z. Q. Zhang, B. White, and G. Papanicolaou, Phys. Rev. Lett. **57**, 1000 (1986).

[20]L. Macon, J. P. Desideri, and D. Sornette (unpublished).